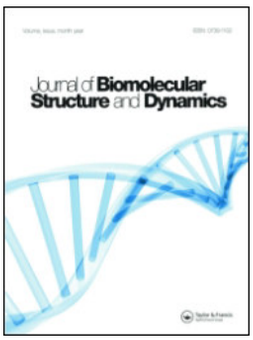

Journal of Biomolecular Structure and Dynamics

ISSN: 0739-1102 (Print) 1538-0254 (Online) Journal homepage: http://www.tandfonline.com/loi/tbsd20

Crystal structure of Staphylococcus aureus Zn-glyoxalase I: new subfamily of glyoxalase I family

Yuri N. Chirgadze, Eugenia A. Boshkova, Kevin P. Battaile, Vitor G. Mendes, Robert Lam, Tiffany S.Y. Chan, Vladimir Romanov, Emil F. Pai & Nickolay Y. Chirgadze

To cite this article: Yuri N. Chirgadze, Eugenia A. Boshkova, Kevin P. Battaile, Vitor G. Mendes, Robert Lam, Tiffany S.Y. Chan, Vladimir Romanov, Emil F. Pai & Nickolay Y. Chirgadze (2018) Crystal structure of Staphylococcus aureus Zn-glyoxalase I: new subfamily of glyoxalase I family, Journal of Biomolecular Structure and Dynamics, 36:2, 376-386, DOI: 10.1080/07391102.2016.1278038

To link to this article: https://doi.org/10.1080/07391102.2016.1278038

Accepted author version posted online: 29 Dec 2016.
Published online: 16 Jan 2017.

Journal of Biomolecular Structure and Dynamics, 2018
Vol. 36, No. 2, 376–386, https://doi.org/10.1080/07391102.2016.1278038

Crystal structure of *Staphylococcus aureus* Zn-glyoxalase I: new subfamily of glyoxalase I family

Yuri N. Chirgadze[a]*, Eugenia A. Boshkova[a], Kevin P. Battaile[b], Vitor G. Mendes[c], Robert Lam[d], Tiffany S.Y. Chan[d], Vladimir Romanov[d], Emil F. Pai[d,e,f,g] and Nickolay Y. Chirgadze[d,h,i]

[a]*Institute of Protein Research, Russian Academy of Sciences, Pushchino 142290, Moscow Region, Russia;* [b]*Advanced Photon Source, Argonne National Laboratory, Hauptman–Woodward Medical Research Institute, IMCA-CAT, Argonne, IL 60439, USA;* [c]*Department of Biochemistry, University of Cambridge, Cambridge CB2 1GA, UK;* [d]*Campbell Family Cancer Research Institute, Ontario Cancer Institute, Princess Margaret Hospital, University Health Network, Toronto, Ontario M5G 2C4, Canada;* [e]*Department of Biochemistry, University of Toronto, Toronto, Ontario M5S 1A8, Canada;* [f]*Department of Molecular Genetics, University of Toronto, Toronto, Ontario M5S 1A8, Canada;* [g]*Department of Medical Biophysics, University of Toronto, Toronto, Ontario M5S 1A8, Canada;* [h]*Department of Pharmacology and Toxicology, University of Toronto, Toronto, Ontario M5S 1A8, Canada;* [i]*X-CHIP Technologies Inc., Toronto, Ontario, Canada*

Communicated by Ramaswamy H. Sarma

(*Received 12 October 2016; accepted 26 December 2016*)

The crystal structures of protein SA0856 from *Staphylococcus aureus* in its apo-form and in complex with a Zn^{2+}-ion have been presented. The 152 amino acid protein consists of two similar domains with α + β topology. In both crystalline state and in solution, the protein forms a dimer with monomers related by a twofold pseudo-symmetry rotation axis. A sequence homology search identified the protein as a member of the structural family Glyoxalase I. We have shown that the enzyme possesses glyoxalase I activity in the presence of Zn^{2+}, Mg^{2+}, Ni^{2+}, and Co^{2+}, in this order of preference. Sequence and structure comparisons revealed that human glyoxalase I should be assigned to a subfamily A, while *S. aureus* glyoxalase I represents a new subfamily B, which includes also proteins from other bacteria. Both subfamilies have a similar protein chain fold but rather diverse sequences. The active sites of human and staphylococcus glyoxalases I are also different: the former contains one Zn-ion per chain; the latter incorporates two of these ions. In the active site of SA0856, the first Zn-ion is well coordinated by His58, Glu60 from basic molecule and Glu40*, His44* from adjacent symmetry-related molecule. The second Zn3-ion is coordinated only by residue His143 from protein molecule and one acetate ion. We suggest that only single Zn1-ion plays the role of catalytic center. The newly found differences between the two subfamilies could guide the design of new drugs against *S. aureus*, an important pathogenic micro-organism.

Keywords: metalloprotein; glyoxalase I; subfamily; pathogen

1. Introduction

Glyoxalase I (*S*-D-lactoylglutathione lyase) is the first of two enzymes of the glyoxalase detoxification system for metabolites derived from glycolysis, such as methylglyoxal and other aldehydes (Aronsson, Marmstal, & Mannervik, 1978; Thornalley, 2003; Vander Jagt, 1989). An increase in the cellular concentration of methylglyoxal can produce toxic effects due to its reactions with DNA, RNA, and proteins (Thornalley, 1996). This protective function of the glyoxalase system makes it an important player in the physiology of the cell. The metabolic pathway of the glyoxalase system is shown in Figure 1. In the first step, cytotoxic aldehyde and glutathione are converted nonenzymatically into nontoxic hemithioacetal, which is turned into thioester *S*-D-lactoylglutathione by glyoxalase I. In the second step, glyoxalase II hydrolyses glutathione thioester to D-lactic acid and glutathione. The glyoxalase system appeared very early in evolution and is found almost universally among all living organisms. The considered enzyme is essential for cell life. It is this important role that makes glyoxalase an attractive drug target, provided that the enzymes from human pathogens can be selectively hit without interference on the human enzyme (Ayoub, Allen, & Thornalley, 1993; Santarius et al., 2010). The structure we report here identifies such a distinctive difference between pathogen and host enzymes.

The enzyme requires a metal ion for catalytic activity. In glyoxalase I from *H. sapiens* and *S. cerevisiae,* the essential ion has been shown to be Zn^{2+} (Aronsson et al., 1978; Cameron, Olin, Ridderstrom, Mannervik, & Jones, 1997). However, glyoxalase I from *E. coli* is completely inactive in the presence of zinc ions (He, Clugston, Honek, & Matthews, 2000). Prokaryotic

*Corresponding author. Email: chir@vega.protres.ru

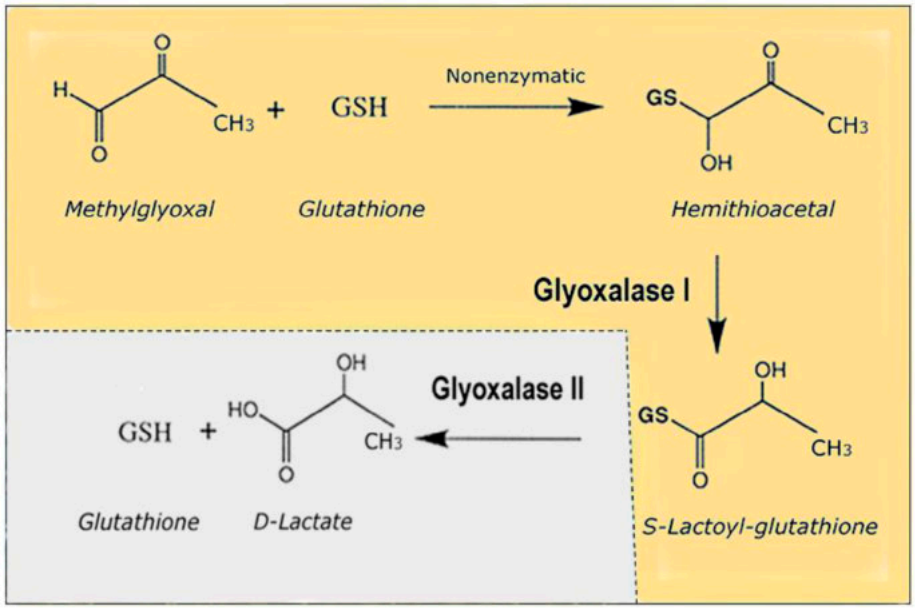

Figure 1. Metabolic pathway of the methylglyoxal detoxifying glyoxalase system. The two enzymes glyoxalase I and II convert methylglyoxal and other aldehyde metabolites of glycolysis to glutathione and D-lactate.

glyoxalase I often prefers a nickel ion but it can also function with zinc, cobalt, manganese, and cadmium (Clugston et al., 1998; Sellin, Eriksson, Aronsson, & Mannervik, 1983; Sellin & Mannervik, 1984; Suttisansanee et al., 2011). This prokaryote/eukaryote distinction may be explained by differences in the metal coordination geometry (He et al., 2000; Sellin et al., 1983). Glyoxalase I molecules exist as homodimers with two pseudo-symmetrical active sites. In all presently known structures of glyoxalase I, the dimeric molecule contains two active sites located inside the large cavities with a single divalent ion inside of each of them. The large cavity is required for accepting the glutathione-hemithioacetal substrate.

The structure of human glyoxalase I was reported in 1997 (Cameron et al., 1997). It was assigned to the glyoxalase I family of metalloproteins that includes two similar domains with βαββββ topology. Based on the similar sequence and structural features, a number of other proteins were also assigned to the 'glyoxalase I like' structural superfamily. It should, however, be noted that these similar tertiary and quaternary structures are also found in bacterial enzymes with other function which permit resistance to antibiotics such as bleomycin (Dumas, Bergdoll, Cagnon, & Masson, 1994). Similarity to glyoxalase I are also found for some unrelated enzymes such as methylmalonyl-CoA epimerase (McCarthy, Baker, Shewry, Patchett, & Baker, 2001), and dioxygenases (Fielding, Kovaleva, Farquhar, Lipscomb, & Que, 2011). Therefore, the full correct and extended name of the 'glyoxalase I like' superfamily is the 'Glyoxalase/Bleomycin resistance protein/Dioxygenase.'

In this communication, we present crystal structures of Zn-glyoxalase I from *Staphylococcus aureus*, taken as gene product SA0856, which belongs to the glyoxalase I structural family. We have found a number of specific features of this structure distinguishing it from already known structures of glyoxalase I. The structure of SA0856, for example, contains two Zn ions in each active site cavity while most of all other known glyoxalase structures contain only one metal ion inside of one active site cavity. As a result, we have suggested a new subfamily B with SA0856 as its representative member. At the same time, other glyoxalase I proteins have been assigned now to subfamily A whose representative member is human glyoxalase I.

2. Material and methods

2.1. Cloning, expression, and purification of recombinant SA0856 protein

The target gene SA0856 was amplified from *S. aureus* genomic DNA by PCR. This DNA fragment was inserted into the Novagen pET15b vector (EMD Millipore, Billerica, MA, USA). Vector containing SA0856 gene in-frame with N-terminal hexahistidine tag was transformed into expression strain *Escherichia coli* BL21 (DE3). Cells were grown on minimal selenomethionine-containing media (Medicilon) supplemented with 50 mg/L Ampicilin in 1 L Tunair flasks at 37 °C to

an OD_{600} of .6, after which the temperature was lowered to 16 °C and IPTG was added to bring the concentration to .5 mM. Expression was allowed to proceed overnight, after which the cells were harvested by centrifugation, flash-frozen in liquid nitrogen, and stored at −80 °C.

Frozen cell pellets were thawed on ice and re-suspended in 100 mM HEPES-Na, pH 7.5, 500 mM NaCl, 5% glycerol, .5% CHAPS, .2 mM TCEP, .1 mM PMSF. After disruption by sonication and centrifugation at 60,000 rpm for 40 min, the lysate was passed through a DE-52 column (2.6 × 7 cm) pre-equilibrated with the same buffer and loaded by gravity flow onto a Ni-NTA column (Qiagen, Germantown, MD, USA). The column was washed with 10 column volumes of wash buffer (50 mM HEPES-Na, pH 7.5, 500 mM NaCl, 5% glycerol, .2 mM TCEP, .1 mM PMSF, 20 mM imidazole) supplemented with .5% CHAPS, followed by 10 column volumes of detergent-free wash buffer and eluted with the same buffer containing 200 mM imidazole.

This eluate was diluted 5-fold with 10 mM Tris-HCl and loaded onto a MonoQ 10/10 column (GE Healthcare) pre-equilibrated with Buffer A (10 mM Tris-HCl, pH 8.0, 100 mM NaCl, .2 mM TCEP). The column was subsequently washed with 2 column volumes of Buffer A and the protein was eluted in a 20 column volume linear gradient from 100 to 500 mM NaCl. Major fractions of the peak containing SA0856 protein were pooled, concentrated using a VIVA-Spin unit (Sartorius NA, Edgewood, NY, USA) and loaded onto a 2.6 × 60 cm Superdex 200 column (GE Healthcare, Mississauga, ON, Canada) equilibrated with 10 mM Tris-HCl, pH 8.0, 150 mM NaCl, .2 mM TCEP. Elution was carried out at a flow rate of 3 mL/min at 8 °C. The SA0856 protein was eluting as an apparent dimer. The final protein sample was concentrated to 30–60 mg/ml, divided into 1.5 mg aliquots, flash-frozen, and stored at −80 °C. The yield was 80–100 mg of pure protein from 4 L of culture.

2.2. Functional activity of glyoxalase I

The glyoxalase I assay was performed as described (Arai, Nihonmatsu-Kikuchi, Itokawa, Rabbani, & Thornalley, 2014). In all cases we have used selenomethionine containing protein. Briefly hemithioacetal was formed by pre-incubating methylglyoxal and glutathione in 50 mM sodium phosphate buffer pH 6.6 for 10 min at 37 °C. The enzyme was then added at the final concentration of 2.5 μM and the reaction observed at 240 nm using a Shimadzu UV-1800 spectrophotometer and heated cuvette block at 37 °C. The effect of the divalent cations Ca^{2+}, Co^{2+}, Mg^{2+}, Mn^{2+}, Ni^{2+}, and Zn^{2+} at 1 mM was also tested. Blank control runs were performed to account for non-enzymatic hemithioacetal isomerization to S-lactoylglutathione. All reagents were purchased from Sigma-Aldrich (St. Louis, MO, USA).

2.3. Crystallization

The protein was thawed and centrifuged at 14,000 rpm in a micro centrifuge for one minute at room temperature. Crystals suitable for X-ray diffraction for apo- and Zn complex structures were obtained after a few days by the sitting drop vapor diffusion method against a 100 μL reservoir solution containing 12–15% PEG3350, 100 mM Mg acetate and 3% ethanol at pH 7.7 in Intelliplates (Hampton Research, Aliso Viejo, CA, USA) incubated at room temperature. Each crystallization drop was set up as a mixture of 1.5 μL of the protein with 1.5 μL reservoir solutions. Zn–SA0856 complex crystals were obtained by co-crystallization method, incubating 2.4 mM of Zn acetate with the protein for one hour prior to crystallization. The crystals were flash-frozen in liquid nitrogen in a solution consisting of mother liquor with 20% ethylene glycol. As a result, the crystals of both apo- and Zn–SA0856 selenomethionine containing proteins were belonged to space group I222 as shown in Table 1.

2.4. Sequence homology search

Homology and sequence conservation of the SA0856 protein were investigated using the protein BLAST search program (Altschul et al., 1997).

2.5. X-ray data collection and processing

X-ray diffraction data-sets for the apo-form of SA0856 and its Zn-complex were collected at a temperature of 100 K on beamline 17-ID at the Advanced Photon Source, Argonne National Laboratory. The diffraction data were reduced using the program autoPROC (Evans, 2006, 2011; Evans & Murshudov, 2013; Kabsch, 2010; Vonrhein et al., 2011). The crystallographic data and refinement statistics are summarized in Table 1.

2.6. Structure determination and crystallographic refinement

Crystals of SA0856 belong to the I222 space group. Coordinates of the SA0856 apo-structure have been deposited in the Protein Data Bank (Lam et al., 2010; PDB ID: 3L20). Phases were determined by the Se-SAD method using the program autoSHARP (Vonrhein, Blanc, Roversi, & Bricogne, 2007). Initial models were generated from experimental density using ARP/wARP (Langer, Cohen, Lamzin, & Perrakis, 2008) followed by refinement with REFMAC (Murshudov, Vagin, & Dodson, 1997; Winn et al., 2011). Both crystal structures were refined with iterative cycles of model building and crystallographic refinement using COOT (Emsley, Lohkamp, Scott, & Cowtan, 2010) and

Table 1. Crystallographic data and refinement statistics.

Data	apo-SA0856	Zn-SA0856
Data collection		
Wavelength (Å)	.97928	1.00
Resolution (Å)	2.45 (2.51–2.45)	2.23 (2.35–2.23)
Space group	I222	I222
Unit cell parameters		
a (Å)	91.7	91.9
b (Å)	93.0	92.6
c (Å)	94.5	95.3
Molecules per asymmetric unit	2	2
Unique reflections	15,138 (1034)	20,144 (2727)
Multiplicity	7.3 (7.2)	6.7 (6.7)
Average $I/\sigma(I)$	9.9 (2.1)	17.6 (2.2)
R_{merge}	.090 (.485)	.065 (.950)
Completeness (%)	99.7 (99.4)	99.8 (100.0)
Refinement and structure statistics		
R_{work}	.209 (.238)	.201 (.265)
R_{free}	.237 (.381)	.234 (.324)
R.m.s.d from ideal geometry		
Bond lengths (Å)	.015	.010
Bond angles (°)	1.528	1.060
Numbers of atoms		
Protein non-H atoms	2402	2379
Water oxygen atoms	28	23
Metal ions	0	4 Zn
Acetate ions	0	2 acetate ions
Ramachandran plot statistics (%)		
Most favored regions	98.2	99.0
Additional allowed regions	1.8	1.0
Disallowed regions	.0	.0

Note: Values in parentheses are for the highest resolution shell.

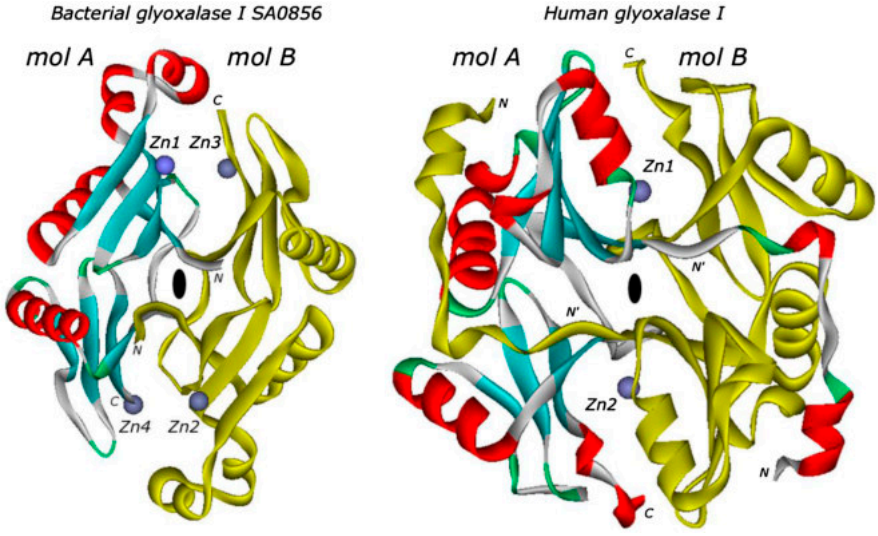

Figure 2. Crystal structures of the Zn-ion complexes of glyoxalase I: the bacterial enzyme SA0856 from *Staphylococcus aureus* and the mammalian one from *Homo sapiens* (Cameron et al., 1997).

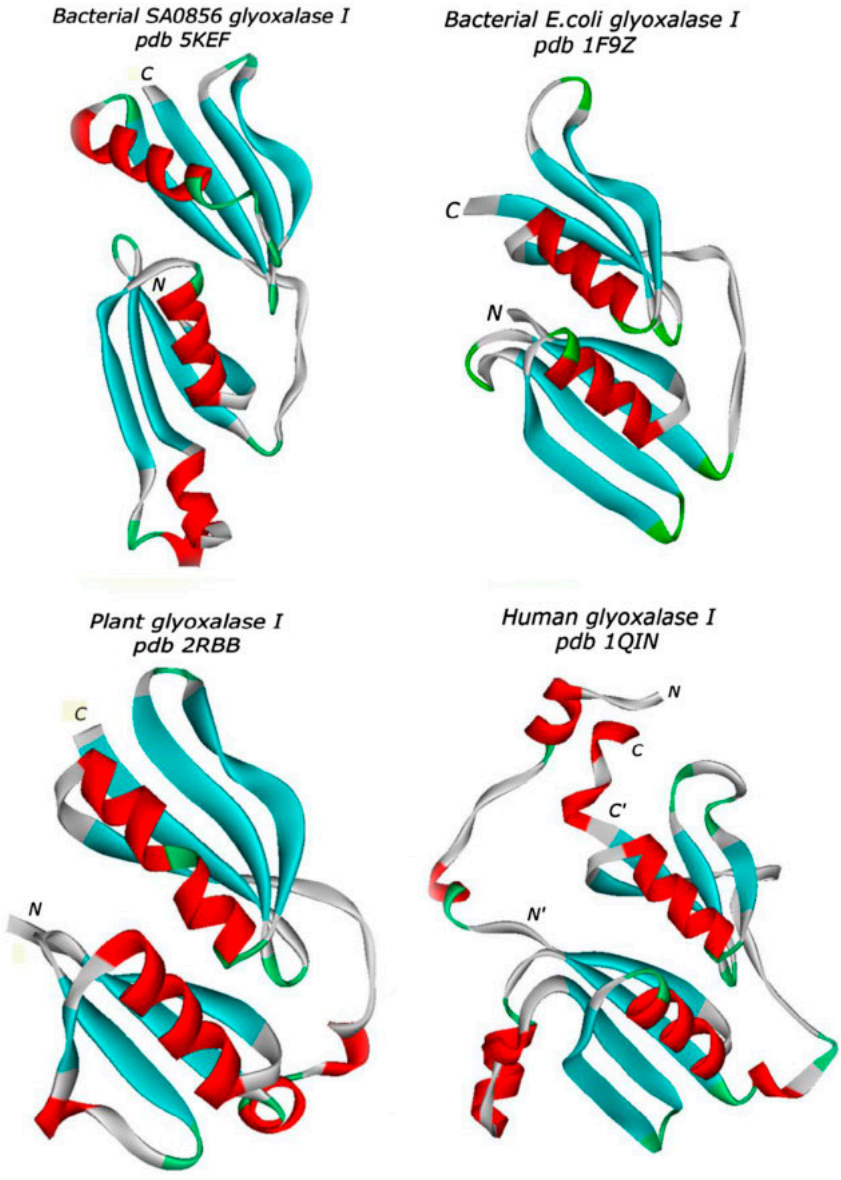

Figure 3. Protein chain folds of the monomers of glyoxalase I from various sources: bacterial enzyme SA0856 from *Staphylococcus aureus*, bacterial enzyme from *Escherichia coli*, plant tomato enzyme from *Burkholderia phytofirmans*, and mammalian enzyme from *Homo sapiens*. Note that the molecule from the human source has extended N- and C-terminal tails.

BUSTER (Bricogne et al., 2011). The Zn-crystal and apo-form are isomorphous with the same space group. We have taken initial phases for Zn-complex crystal from the crystal of apo-protein. Coordinates of four Zn ions were obtained independently from the very clear peaks of the Zn anomalous difference map. They were input in the model at the later stages of refinement after most of the protein model was built. Water molecules as well as other solvent ligands were added based on the $2mF_o$ $-DF_c$ map in COOT and subsequently refined with BUSTER. The refinement statistics are listed in Table 1.

2.7. Determination of interatomic contacts between monomers

The interatomic contacts in the protein dimer were analyzed with the help of the DimPlot program, part of the program suites LigPlot + and LIGPLOT (Wallace, Laskowski, & Thornton, 1996).

3. Results

3.1. Protein structure

The Zn complex of protein SA0856 contains 152 amino acids and consists of two similar monomers with very

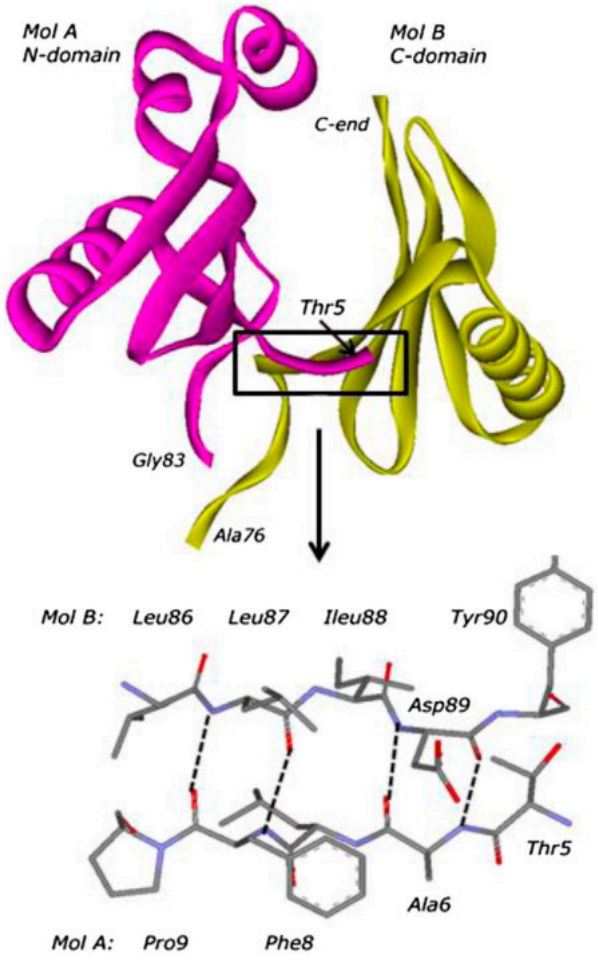

Figure 4. Beta-sheet clip between monomers A and B. The stretches of chains lock together both monomers in the dimer of Zn-glyoxalase I from *S. aureus*.

similar structures and topologies of two-layer $\alpha + \beta$ sandwiches. In the crystalline state as well as in solution the protein exists as a dimer with the monomers related by a twofold pseudo symmetry rotation axis. Each monomer contains the topologically equivalent N- and C-domains, with 70 and 74 residues, respectively, visible in the electron density map.

Each dimer contains two large, symmetry-related cavities in which Zn-ions are located (Figure 2). As shown in this figure, the main chain topology and the overall structure of bacterial SA0856 are similar to those of human glyoxalase I, with the exception of two additional NN′- and CC′-terminal segments in the human enzyme. Thus, we assign the SA0856 to the superfamily of 'glyoxalase I like' proteins. To be more accurate, it belongs to the structural superfamily '*Glyoxalase/Bleomycin resistance protein/Dioxygenase*.' In order to determine the function of SA0856, we tested the protein for enzymatic activity. Glyoxalase I activity has been be confirmed (see Section 3.4). In contrast to human glyoxalase, which binds one Zn-ion in each active site, the bacterial enzyme SA0856 contains two per monomer. It should be noted that glyoxalase I in all crystal structures determined so far contains one metal atom per active site cavity, in the many cases a Zn-ion. The extended terminal ends in the structure of human glyoxalase I suggest an increase in the stability of the dimer molecule because these peptide ends bind additionally the monomers A and B of the dimer.

Cartoons of the folds of various glyoxalase I monomers are shown in Figure 3, representing two bacterial (*S. aureus* and *E. coli*), plant (tomato), and mammalian (human) sources. Despite some minor differences, the topology and domain structures are very similar. In particular, each domain has a common basic topology motif βαββββ.

A dimeric state seems to be essential for SA0856's biological activity because each active site is formed by two polypeptide chains. The enzyme's stability is caused by the numerous hydrophobic contacts between protomers and by several H-bonds. We identified about 120 hydrophobic contacts between nonpolar atoms and 25 H-bonds at the subunit–subunit interface. Structurally most interesting are seven paired H-bonds, which form beta-sheet fixing clip between both monomers as shown in Figure 4. In fact, we have observed also another symmetry equivalent analog of this structure.

3.2. *Sequence and structural homology*

Sequence analysis of the glyoxalase I family revealed SA0856 as homologous to its members and therefore should be considered a member, too. We have showed that the sequences could be divided into two distinctly separate subfamilies. Subfamily A, with its representative structure glyoxalase I from *H. sapiens* (Cameron et al., 1997), includes some enzymes from various organisms from bacteria to plants and mammals. Subfamily B, with its newly elucidated representative structure SA0856 from *S. aureus,* includes proteins from various bacteria; so far all presented here are gram-positive. The functions of those proteins are yet unknown. However, this study suggests their assigning to subfamily B of the glyoxalase I family.

The sequences of these subfamilies are presented in Figure 5. All sequences have been divided in two different subfamilies with representative glyoxalase I proteins from *H. sapiens* (pdb 1QIN) for subfamily A, and from *S. aureus* (pdb 5KEF) for subfamily B, correspondingly. Averaged pair sequence identity values in both subfamilies are rather low and equal to, in %, as follows:

	N-domain	C-domain
Subfamily A	25.7	18.3
Subfamily B	30.0	25.4

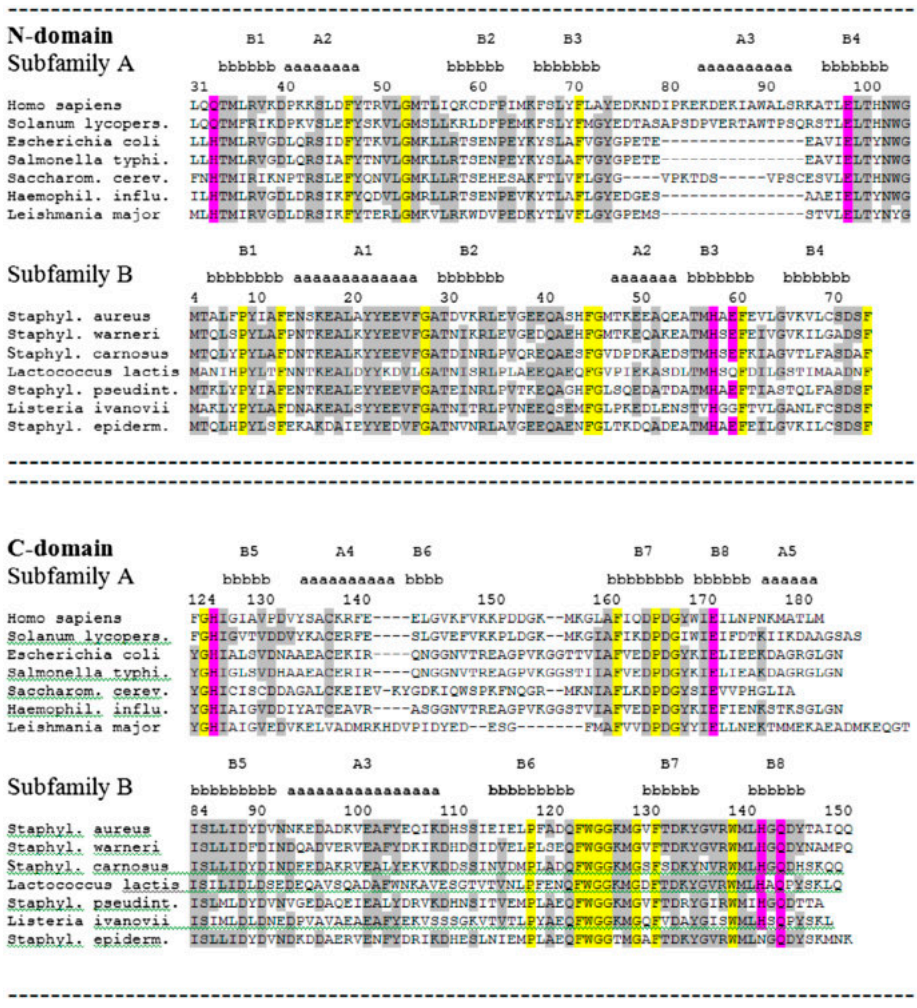

Figure 5. Sequence alignment and homology of bacterial sequences belonging to different subfamilies A and B of the glyoxalase I family. The conserved residue positions with identities 70–100% are shown against the gray background. Topology essential and structure-specific residues are marked in yellow color. Catalytic residues coordinated metal ions are shown in magenta.

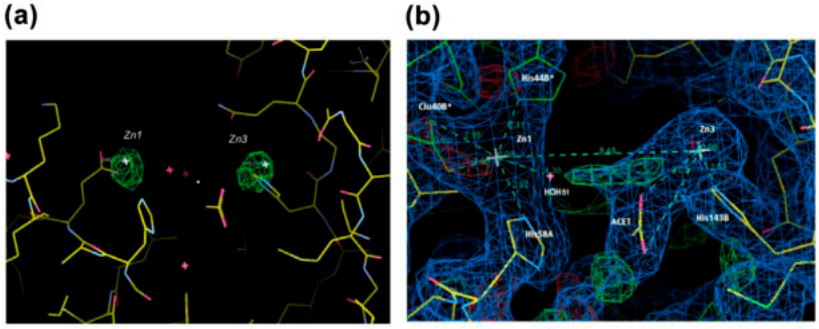

Figure 6. Electron density maps of the *S. aureus* Zn–SA0856 complex in the region of the Zn-ions. (a) Zn anomalous difference Fourier map with bright green Zn densities shows two Zn ions locations; density peak heights are about 5 sigma. Model of dimer molecule of glyoxalase I SA0856 with water molecules (red crosses) are also superimposed on the same map. (b) Electron density map in the region of the Zn1 and Zn3 ions is shown in blue; a difference ($F_o - F_c$) Fourier map is shown in green (positive) and red (negative). Protein basic molecule is shown partially in yellow sticks, and adjacent symmetry-related molecule (*) is drawn partially in green sticks.

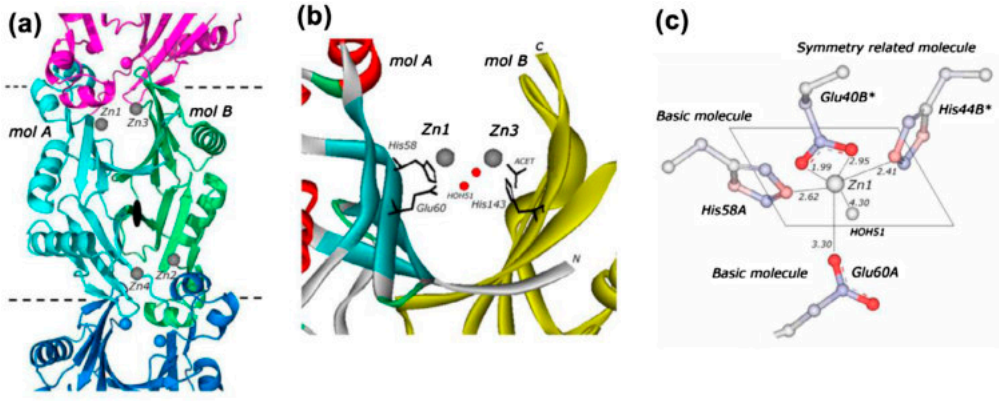

Figure 7. Crystal structures of the *S. aureus* Zn–SA0856 glyoxalase I. (a) Crystal packing of protein dimers. (b) Active site cavity of the Zn–SA0856 dimer, two small red spheres indicate the positions of the fixed structural water molecules. (c) Configuration of coordinated atomic groups around the Zn1-ion.

Table 2. Contact distances of Zn1 and Zn3 with coordinated ligands in active site cavity of Zn-glyoxalase I SA0856 from *S. aureus.*

Contact atomic pairs	Distance (Å)
Zn1 – NE2 His 58A	2.62
Zn1 – OE2 Glu 60A	3.30
Zn1 – OE1 Glu 40B*	1.99
Zn1 – OE2 Glu 40B*	2.95
Zn1 – NE2 His 44B*	2.41
Zn1 – HOH 51	4.30
Zn3 – NE2 His 143B	2.52
Zn3 – NE2 Gln 145B	5.71
Zn3 – O ACT	3.03
Zn3 – OXT ACT	4.54

Notes: A and B – two protein molecules, which form dimer of glyoxalase I.
Asterisk designates an adjacent crystallographic symmetry-related molecule, which form intermolecular contacts in crystal medium.

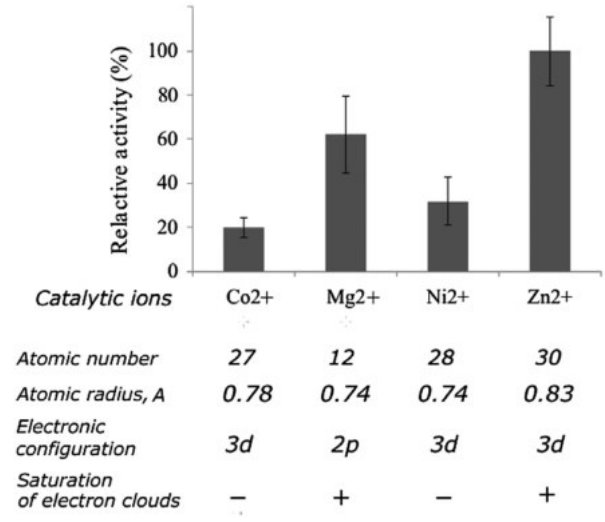

Figure 8. Relative activity of *Staphylococcus aureus* glyoxalase I SA0856 in the presence of Zn^{2+}, Mg^{2+}, Ni^{2+}, and Co^{2+} ions, that play a role of catalytic center for this enzyme.

The conserved residue positions, with identity values higher than 70%, are shown here against the gray background. The topology essential and structure-specific residues, such as Gly, Pro, Leu, Phe, Trp, are marked in yellow color, and catalytic residues coordinating metal ions are shown in magenta. The subfamily B displays larger identity values of regular regions. These are localized in regions of α-helix A1 and β-sheet B3 (N-domain) and in regions of β-sheets B7 and B8 (C-domain). The most distinctive in two families are the differences in the positioning of Zn-coordinated residues in two subfamilies which are located both in N- and C-domains (Figure 5).

3.3. *Active site structure*

Electron density maps of the Zn–SA0856 complex in the region of the Zn1 and Zn3 ions are shown in Figure 6. Here, Zn anomalous differences Fourier map with bright green densities presents direct experimental prove of four Zn ions locations. Detailed electron density maps shows coordination spheres around Zn1 and Zn3 ions.

In the crystalline state, intermolecular contacts were revealed with adjacent crystallographic symmetry-related molecules (Figure 7(a)). The most significant contacts occur at the points where neighboring molecules penetrate into the large active site cavities. One of two such cavities of the Zn-glyoxalase I for an isolated dimer molecule is shown in Figure 7(b). The first Zn1 is well coordinated by His58A, Glu60A from basic molecule and Glu40B*, His44B* from adjacent symmetry-related (*) molecule. In contrast, the second Zn3-ion of this cavity is coordinated only by residue His143B from basic molecule and one fixed acetate ion from solution. The NE2 atom of second

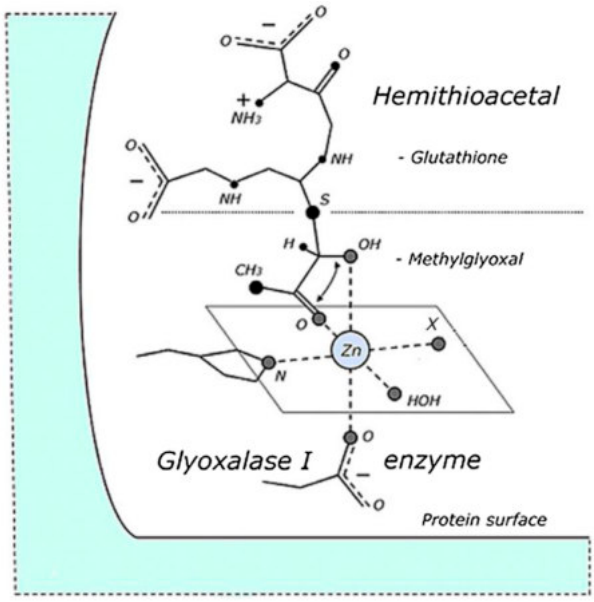

Figure 9. Sketch of a hypothetical binding of hemithioacetal, the product of glutathione binding to methylglyoxal. It was based on the Zn ion location in the active site of the glyoxalase I enzyme, where Zn1 ion has the catalytic octahedral configuration. One can postulate that the proton attacks CO or OH groups of the methylglyoxal part of hemithioacetal leads to rearrangement of these bonds. Letter X designates undefined solution ion, water molecule or closing residue of the protein.

nearest residue Gln145B was revealed at distance 5.71 Å. No other contacts of Zn3 with symmetry-related molecules were revealed. The distance between Zn1 and Zn3 was measured as equal to 8.48 Å.

Details of Zn1 and Zn3 with coordinated ligands are presented in Figure 7(c) and the contact distances in Table 2. For Zn1, the majority of distances are in the range 2.00–3.30 Å and only oxygen atom of important fixed structural water HOH51 is removed at 4.30 Å. For Zn3 there are a limited number of ligands His143B, Gln145B and fixed acetate ion are revealed in the range 2.50–5.71 Å. Three contact distances are larger the value of maximum contact limit, equal to about 3.0–3.3 Å. But such a contact distance values could be smaller in the solution due the mobility of the protein structure.

Second ion pair Zn2–Zn4 is nearly symmetry related to the Zn1–Zn3 one. The coordination sphere of ion Zn2 (analog of Zn1) is very similar to that of Zn1 with nitrogen atoms of His58B, His44A*, and carboxylic group of Glu40A*. However, the surroundings of Zn4 (analog of Zn3) are different. We have observed only one contact of Zn4 with His143A at a distance of 2.28 Å. The acetate ion is absent here, and the role of the counter ions may play some quickly exchangeable solution ions or water molecules.

Zn1, and symmetry equivalent Zn2, are the only Zn-ions with a most complete coordination sphere, which makes it a good candidate for a catalytic center. Three atoms of His58A, Glu40B*, His44B* and the oxygen of water HOH51 are located approximately in one plane that also contains the Zn-ion (Figure 7(c)). An oxygen atom of Glu60A occupies one of the lower positions whereas the sixth coordination position remains empty. We strongly suggest that only a single Zn1 (Zn2)-ion could play the role of catalytic center for SA0856 glyoxalase I.

3.4. *Glyoxalase activity of SA0856 with different metal ions*

The enzyme exhibited glyoxalase I activity in the presence of Zn^{2+}, Mg^{2+}, Ni^{2+}, and Co^{2+} in order of preference (Figure 8). No activity is detected in the presence of Ca^{2+} and Mn^{2+} ions. It is also observed that the enzyme is strictly dependent of these divalent cations, since no activity is observed in the absence of cations. Most significant values of activities 100 and 60%, correspondingly, were observed for Zn^{2+} and Mg^{2+} ions. These ions have different configurations of electron clouds that differ in geometry of their coordination spheres. However, higher activities of these ions in comparison with Ni^{2+} and Co^{2+} ions may be also explained by the completed saturation of higher electronic levels with electrons as shown in the Figure 8.

4. Discussion and conclusion

The most important result of this communication is the identification of two different subfamilies of glyoxalase I sequences. Subfamily A is described by its representative, the structurally already well-known enzyme from *H. sapiens* (Cameron et al., 1997). The subfamily includes homologous enzymes from a broad selection of organisms: bacteria, plants, and mammals. The existence of subfamily B was discovered when the new crystal structure of the bacterial glyoxalase I from *S. aureus* was elucidated. It now represents the original enzyme type for subfamily B. This subfamily presently includes only enzymes from gram-positive bacteria. The three-dimensional structure of Zn-glyoxalase I from *S. aureus* suggests that all seven known homologs can be assigned to subfamily B. The suggested functions of these proteins must be confirmed.

Another valuable result is the knowledge of the fold and active site of the new Zn-ion saturated crystal structures of the glyoxalase I SA0856 from the pathogenic bacterium *S. aureus*. The structure differs significantly from those glyoxalase I whose three-dimensional structures are already known. The main features of the *S. aureus* enzyme are a larger active site and the presence of two, instead of one, metal ions at each of the binding sites. However, we have seen that only one Zn1-ion can play the role of catalytic center.

Formed from methylglyoxal to glutathione, hemithioacetal is the substrate of glyoxalase I. Based on the structures presented in this communication, Figure 9 shows a sketch of a possible interaction between this substrate and the Zn-center of the *S. aureus* enzyme. There should also be interactions between other charged residues of hemithioacetal and the protein surface. It is immediately obvious that the presence of a more complex molecule containing glutathione residue as part of the substrate requires a large room in active site cavity.

Protein glyoxalase I SA0856 is essential for survival of the pathogenic bacterium *S. aureus* (Thornalley, 2003). Detailed knowledge of its overall fold and especially the structure of its active site is important to determine whether the differences to the host homolog are sufficient to allow specific targeting for drugs. The data obtained are a step on this way. One could hope that it help to both, overall medical practice, and patient care.

Acknowledgements

We express our gratitude to Prof. Tom Blundell, FRS, and Dr. Dmitri Chirgadze, Cambridge University, UK, for their valuable help and support in performing activity assays of Zn-glyoxalase I. EFP acknowledges support from the Canada Research Chairs program. Contract grant sponsors: Ontario Research and Development Challenge Fund (contract No. 99-SEP-0512). Use of the IMCA-CAT beam line 17-ID at the Advanced Photon Source was supported by the companies of the Industrial Macromolecular Crystallography Association through a contract with the Hauptman-Woodward Medical Research Institute. This research used resources of the Advanced Photon Source, a US Department of Energy Office of Science User Facility operated for the DOE Office of Science by Argonne National laboratory under contract No. DE-AC02-06CH11357.

Disclosure statement

No potential conflict of interest was reported by the authors.

Funding

This work was financially supported by Ontario Research and Development Challenge Fund [grant number 99-SEP-0512]; Argonne National laboratory under [grant number DE-AC02-06CH11357].

References

Altschul, S. F., Madden, T. L., Schäffer, A. A., Zhang, J., Zhang, Z., Miller, W., & Lipman, D. J. (1997). Gapped BLAST and PSI-BLAST: A new generation of protein database search programs. *Nucleic Acids Research, 25*, 3389–3402.

Arai, M., Nihonmatsu-Kikuchi, N., Itokawa, M., Rabbani, N., & Thornalley, P. J. (2014). Measurement of glyoxalase activities. *Biochemical Society Transactions, 42*, 491–494.

Aronsson, A. C., Marmstal, E., & Mannervik, B. (1978). Glyoxalase I, a zinc metalloenzyme of mammals and yeast. *Biochemical and Biophysical Research Communications, 81*, 1235–1240.

Ayoub, F. M., Allen, R. E., & Thornalley, P. J. (1993). Inhibition of proliferation of human leukemia 60 cells by methylglyoxal *in vitro*. *Leukemia Research, 17*, 397–401.

Bricogne, G., Blanc, E., Brandl, M., Flensburg, C., Keller, P., Paciorek, W., … Womack, T. O. (2011). BUSTER *(Version 2.10.0, Ed.)*. Cambridge: Global Phasing Ltd.

Cameron, A. D., Olin, B., Ridderstrom, M., Mannervik, B., & Jones, T. A. (1997). Crystal structure of human glyoxalase I – Evidence for gene duplication and 3D domain swapping. *The EMBO Journal, 16*, 3386–3395.

Clugston, S. L., Barnard, J. F. J., Kinach, R., Miedema, D., Ruman, R., Daub, E., & Honek, J. F. (1998). Overproduction and characterization of a dimeric non-zinc glyoxalase I from *Escherichia coli*: Evidence for optimal activation by nickel ions. *Biochemistry, 37*, 8754–8763.

Dumas, P., Bergdoll, M., Cagnon, C., & Masson, J. M. (1994). Crystal structure and site-directed mutagenesis of a bleomycin resistance protein and their significance for drug sequestering. *The EMBO Journal, 13*, 2483–2492.

Emsley, P., Lohkamp, B., Scott, W. G., & Cowtan, K. (2010). Features and development of Coot. *Acta Crystallographica, D66*, 486–501.

Evans, P. R. (2006). Scaling and assessment of data quality. *Acta Crystallographica, D62*, 72–82.

Evans, P. R. (2011). An introduction to data reduction: Space-group determination, scaling and intensity statistics. *Acta Crystallographica, D67*, 282–292.

Evans, P. R., & Murshudov, G. N. (2013). How good are my data and what is the resolution? *Acta Crystallographica, D69*, 1204–1214.

Fielding, A. J., Kovaleva, E. G., Farquhar, E. R., Lipscomb, J. D., & Que, L. (2011). A hyperactive cobalt-substituted extradiol-cleaving catechol dioxygenase. *JBIC Journal of Biological Inorganic Chemistry, 16*, 341–355.

He, M. M., Clugston, S. L., Honek, J. F., & Matthews, B. W. (2000). Determination of the structure of *Escherichia coli* glyoxalase I suggests a structural basis for differential metal activation. *Biochemistry, 39*, 8719–8727.

Kabsch, W. (2010). XDS. *Acta Crystallographica, D66*, 125–132.

Lam, R., Chan, T., Battaile, K. P., Mihajlovic, V., Romanov, V., Soloveychik, M., … Chirgadze, N. Y. (2010). *Crystal structure of a hypothetical protein from* Staphylococcus aureus. RCSB PDB, PDB ID: 3L20.

Langer, G., Cohen, S. X., Lamzin, V. S., & Perrakis, A. (2008). Automated macromolecular model building for X-ray crystallography using ARP/wARP version 7. *Nature Protocols, 3*, 1171–1179.

McCarthy, A. A., Baker, H. M., Shewry, S. C., Patchett, M. L., & Baker, E. N. (2001). Crystal structure of methylmalonyl-coenzyme A epimerase from *P. shermanii*: A novel enzymatic function on an ancient metal binding scaffold. *Structure, 9*, 637–646.

Murshudov, G. N., Vagin, A. A., & Dodson, E. J. (1997). Refinement of macromolecular structures by the maximum-likelihood method. *Acta Crystallographica, D53*, 240–255.

Santarius, T., Bignell, G. R., Greenman, C. D., Widaa, S., Chen, L., Mahoney, C. L., … Stratton, M. R. (2010). GLO1 – A novel amplified gene in human cancer. *Genes, Chromosomes & Cancer, 49*, 711–725.

Sellin, S., Eriksson, L. E. G., Aronsson, A. C., & Mannervik, B. (1983). Octahedral metal coordination in the active site of glyoxalase I as evidenced by the properties of Co(II)-glyoxalase I. *Journal of Biological Chemistry, 258*, 2091–2093.

Sellin, S., & Mannervik, B. (1984). Metal dissociation constants for glyoxalase I reconstituted with Zn^{2+}, Co^{2+}, Mn^{2+}, and Mg^{2+}. *Journal of Biological Chemistry, 259*, 11426–11429.

Suttisansanee, U., Lau, K., Lagishetty, S., Rao, K. N., Swaminathan, S., Sauder, J. M., … Honek, J. F. (2011). Structural variation in bacterial glyoxalase I enzymes: Investigation of the metalloenzyme glyoxalase I from clostridium acetobutylicum. *Journal of Biological Chemistry, 286*, 38367–38374.

Thornalley, P. J. (1996). Pharmacology of methylglyoxal: Formation, modification of proteins and nucleic acids, and enzymatic detoxigfication – A role in pathogenesis and antiproliferative chemotherapy. *General Pharmacology: The Vascular System, 27*, 565–573.

Thornalley, P. J. (2003). Glyaxalase I – Structure, function and critical role in the enzymatic defence against glycation. *Biochemical Society Transactions, 31*, 1343–1348.

Vander Jagt, D. L. (1989). The glyoxalase system. In D. Dolphin, R. Poulson, & O. Avramovic (Eds.), *Glutathione: Chemical, biochemical and medical aspects. Part A* (pp. 597–641). New York, NY: Wiley.

Vonrhein, C., Blanc, E., Roversi, P., & Bricogne, G. (2007). Automated structure solution with autoSHARP. *Methods in Molecular Biology, 364*, 215–230.

Vonrhein, C., Flensburg, C., Keller, P., Sharff, A., Smart, O., Paciorek, W., … Bricogne, G. (2011). Data processing and analysis with the autoPROC toolbox. *Acta Crystallographica, D67*, 293–302.

Wallace, A. C., Laskowski, R. A., & Thornton, J. M. (1996). LIGPLOT: A program to generate schematic diagrams of protein-ligand interactions. *Protein Engineering, 8*, 127–134.

Winn, M. D., Ballard, C. C., Cowtan, K. D., Dodson, E. J., Emsley, P., Evans, P. R., … Wilson, K. S. (2011). Overview of the CCP4 suite and current developments. *Acta Crystallographica, D67*, 235–242.